Single-molecule tracking of small GTPase Rac1 uncovers spatial regulation of membrane translocation and mechanism for polarized signaling

Sulagna Das, Taofei Yin, Qingfen Yang, Jingqiao Zhang, Yi I. Wu, and Ji Yu[1]

Center for Cell Analysis and Modeling, University of Connecticut Health Center, Farmington, CT 06030

Edited by Martin A. Schwartz, Yale School of Medicine, New Haven, CT, and accepted by the Editorial Board December 10, 2014 (received for review June 30, 2014)

Polarized Rac1 signaling is a hallmark of many cellular functions, including cell adhesion, motility, and cell division. The two steps of Rac1 activation are its translocation to the plasma membrane and the exchange of nucleotide from GDP to GTP. It is, however, unclear whether these two processes are regulated independent of each other and what their respective roles are in polarization of Rac1 signaling. We designed a single-particle tracking (SPT) method to quantitatively analyze the kinetics of Rac1 membrane translocation in living cells. We found that the rate of Rac1 translocation was significantly elevated in protrusions during cell spreading on collagen. Furthermore, combining FRET sensor imaging with SPT measurements in the same cell, the recruitment of Rac1 was found to be polarized to an extent similar to that of the nucleotide exchange process. Statistical analysis of single-molecule trajectories and optogenetic manipulation of membrane lipids revealed that Rac1 membrane translocation precedes nucleotide exchange, and is governed primarily by interactions with phospholipids, particularly PI(3,4,5)P_3, instead of protein factors. Overall, the study highlights the significance of membrane translocation in spatial Rac1 signaling, which is in addition to the traditional view focusing primarily on GEF distribution and exchange reaction.

RhoGTPase | sptPALM | cell polarization | Rac1 | super-resolution microscopy

Cell polarization is critical for many biological processes, such as front–rear polarity during directed cell migration (chemotaxis, haptotaxis, wound healing, etc.), apical–basal polarity in epithelial cells, and axon specification in neuronal cells. The asymmetric distribution of signaling molecules, adhesion components, and cytoskeletal structures is important for the establishment of polarization. Among signaling proteins, the Rho family small GTPase Rac1 is ubiquitously required for cytoskeletal changes leading to a polarized morphology in many cells (1–4).

Most small GTPases function as molecular switches, cycling between a GTP-bound active state and a GDP-bound inactive state. Activation of small GTPases typically requires guanine nucleotide exchange factors (GEFs) that promote the exchange of GDP for GTP. Inactivation requires the inherent GTPase activity, enhanced by the GTPase Activating Proteins (GAPs) (5, 6). Thus, each Rac1 molecule continuously cycles between the active and inactive state during their intracellular existence.

Besides the guanine nucleotide binding cycle, another cycle that governs Rac1 activity is the membrane/cytoplasm translocation cycle. Rac1 GTPase, as with many other small GTPases, is posttranslationally prenylated at its C terminus and is capable of binding to lipid bilayers (7, 8). Under basal conditions, the majority of Rac1 localizes to the cytoplasm in complex with RhoGDI molecules, which block its interactions with GEFs and GAPs and its downstream effectors (9–12). To become active, Rac1 needs to translocate to the membrane and be free from RhoGDI binding, allowing for its activation by GEFs and its interaction with effectors (6, 10). The guanine nucleotide state of Rac1 and other highly homologous Rho GTPases has been studied with high spatial–temporal detail using various FRET (fluorescence resonance energy transfer) sensors (13–16). In contrast, relatively little is known about the spatial–temporal regulation of the Rac1 membrane translocation cycle, owing to the difficulty in accurately quantifying the concentration of Rac1 on the membrane.

Membrane-bound Rac1 typically represents only a very small fraction of the total protein, with the majority of Rac1 in the cytosol (17). Thus, ensemble measurements of fluorescently labeled Rac1, even with the "membrane-selective" techniques such as total internal reflection fluorescence microscopy (TIRFM), can have significant contributions from the cytosolic pool. A second problem with TIRFM is that the distance between the plasma membrane to the substrate may vary within the same cell and thus contribute to intensity variations.

To address these problems, we took a single-particle tracking Photoactivation Localization Microscopy (sptPALM) approach (18–20) to track the temporal trajectories of individual Rac1 molecules in cells. By confining the analysis to molecules that are undergoing 2D instead of 3D free diffusion (Fig. 1*A*), the subpopulation of membrane-bound Rac1 molecules was reliably identified. We performed further quantification of the membrane recruitment kinetics by directly counting the number of mole-

Significance

Rac1 activation involves two steps: translocation to plasma membrane and nucleotide exchange. Most previous studies focused on the nucleotide exchange cycle. Here we sought to understand membrane translocation dynamics by developing a single-particle tracking-based method. The labeled Rac1 molecules were further adapted for simultaneous FRET sensing of Rac1 nucleotide state, enabling a simultaneous comparison between Rac1 translocation dynamics and its nucleotide exchange dynamics. Elevated membrane recruitment can contribute significantly to polarized Rac1-signaling. This finding draws attention to the importance of spatial regulation of the Rac1 translocation process in the regulation of RhoGTPase signaling. Rac1 recruitment to membrane precedes its interaction with protein factors (e.g., GEFs) and is governed by phospholipid distributions. This finding resolves a long-standing question of the mechanism of Rac1 activation.

Author contributions: S.D., Y.I.W., and J.Y. designed research; S.D., T.Y., and Q.Y. performed research; T.Y., Y.I.W., and J.Y. contributed new reagents/analytic tools; S.D. and J.Z. analyzed data; and S.D., Y.I.W., and J.Y. wrote the paper.

The authors declare no conflict of interest.

This article is a PNAS Direct Submission. M.A.S. is a guest editor invited by the Editorial Board.

[1]To whom correspondence should be addressed. Email: jyu@uchc.edu.

This article contains supporting information online at www.pnas.org/lookup/suppl/doi:10.1073/pnas.1409667112/-/DCSupplemental.

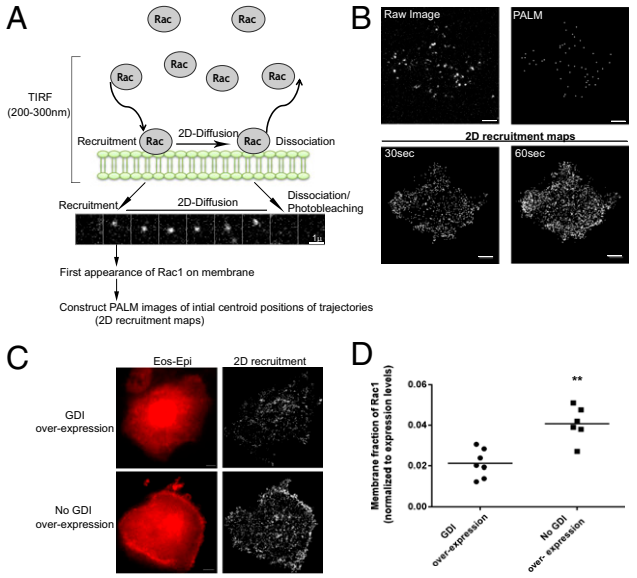

Fig. 1. Detection of membrane recruitment of Rac1 by sptPALM. (*A*) Schematic of the single-molecule detection and interpretation. Under continuous illumination with 562-nm light, photoconverted Eos-Rac1 molecules recruited to the membrane were detected as spatially segregated fluorescent spots, which then undergo 2D membrane diffusion (montage shown). The disappearance of the molecule is either due to dissociation from the membrane or photobleaching of the fluorophore. This represents the membrane translocation cycle of Rac1 from cytosol. The first appearance of a molecule on the membrane is recorded as a recruitment event. (*B*) The raw fluorescent image of Eos-wtRac1 and the corresponding PALM image of the molecule. The 2D recruitment maps for two different time points (30 s and 60 s) generated by fitting the initial centroid position of all molecules lasting 300 ms or more. (*C*) Wide-field epifluorescence images and 2D recruitment maps of activated Eos-wtRac1 molecules in cells cotransfected with wtRac1 and RhoGDI or wtRac1 alone. (*D*) Graph showing the membrane fraction of wtRac1 (from 2D recruitment maps) normalized to total Rac1 expression level (from Eos epifluorescence images). Scale bar corresponds to 5 μm. $^{**}P < 0.005$. Data pooled from three independent experiments, GDI overexpression (seven cells, 3.5×10^4 trajectories), and no GDI overexpression (six cells, 4.2×10^4 trajectories).

cules, instead of relying on the intensity of microscopy images, and therefore the quantification is insensitive to membrane/substrate distances. With these single-molecule analyses, we discovered that membrane recruitment of Rac1 is a spatially regulated process and is associated with protrusions exhibiting high Rac1 activity. In combination with FRET imaging in the same cells, our single-particle tracking (SPT) measurements, further allowed us to delineate the translocation and nucleotide exchange cycles. We also investigated the mechanism of polarized Rac1 recruitment via imaging and optogenetic approaches, and demonstrated that spatial regulation of Rac1 recruitment occurs via a protein–lipid interaction, primarily by a polarized $PI(3,4,5)P_3$ gradient in the cells.

Results

SPT Method for Studying Rac1 Membrane Translocation. To identify membrane-bound Rac1 molecules, we labeled Rac1 with a photoconvertible Eos tag (21) and expressed the construct in MCF7 cells. Pulldown experiments confirmed that Eos-Rac1 undergoes activation and can interact with its effector p21 activated kinase (PAK) (Fig. S1*A*). Using the sptPALM technique (22), a fraction of Eos was photoactivated with UV light, and, single molecules of Eos-Rac1 bound to the plasma membrane and undergoing 2D diffusive motion were detected by TIRF (total internal reflection fluorescence) illumination (Movie S1). The appearance of a molecule was used to identify an initial membrane binding event. The disappearance of fluorescent molecules can be attributed to the photobleaching of the fluorophore Eos, since the average trajectory duration of Eos-Rac1 ($\tau = 0.485$) was comparable to that of pm-Eos (Eos with Lyn *N*-term sequence) (23) (Fig. S1*B*). This suggests that the actual Rac1 membrane dissociation rates are slower than the rate of photobleaching under our imaging conditions. The measurements of the membrane recruitment kinetics of Rac1 are, however, independent of the photobleaching properties of Eos.

To visualize the spatial distribution of membrane recruitment events, we constructed pseudo-PALM images using only the initial centroid location of each single-molecule trajectory, which we refer to as a 2D recruitment map (Fig. 1*B*). Each point in the map signifies a single recruitment event. We found that the number of molecules detected over 1 min is generally sufficient for visualizing the spatial distribution of the recruitment rates (Figs. 1*B* and 2). Since most cellular processes involving Rac1 activation happen at a time scale of minutes, SPT-based assays are suitable for studying these processes. Moreover, we also examined PALM images where all positions of Rac1 trajectories are plotted (Fig. S1*D*). We found that these PALM images closely resemble the 2D recruitment maps (Fig. S1 *C*–*E*), suggesting that Rac1 molecules remain within local regions after recruitment and the location of Rac1's initial recruitment is pertinent to the spatial aspects of Rac1 signaling.

Previous studies have shown that overexpressing RhoGDI significantly alters Rac1 recruitment dynamics and reduces the number of membrane-bound Rac1 molecules (17). Therefore, to validate our SPT-based method, we investigated whether the SPT measurements can recapitulate the regulation of Rac1 by RhoGDI. In cells overexpressing RhoGDI, although we still detect membrane-bound individual Rac1 molecules, the number was lower than control cells in the same experimental setup (Fig. 1*C*). By computing the recruitment frequency normalized to the integrated intensity of the epifluorescence image (Fig. 1 *C* and *D*), we verified that RhoGDI overexpressing cells had significantly lower relative recruitment rates.

Finally, we carried out SPT experiments on the RhoGDI molecule itself (Movie S2), by expressing Eos-labeled RhoGDI molecules. We found that, unlike Rac1, RhoGDI molecules did not exhibit any 2D diffusion at the time scale of our experiments, suggesting that the interaction between RhoGDI and membrane-bound Rac1, if it exists at all, is very transient.

Rac1 Recruitment Rate Is Elevated in Membranes of Cell Protrusions. To examine whether the translocation of Rac1 to the membrane is a spatially regulated process, we carried out SPT measurements on MCF7 cells during cell spreading on collagen substrate, a condition that activates Rac1 (17, 24, 25). Isolated MCF7 cells were seeded onto glass coverslips coated with type I collagen to initiate cell spreading, and single molecules of Rac1 molecules were imaged during the process (Fig. 2*A*). A large number of Rac1 molecules were recruited to the plasma membrane as seen in the 2D recruitment maps (Fig. 2*A*). While recruitment events could be detected throughout the cell area, an elevated recruitment or on-rate was apparent within 5 μm from the leading edges of membrane protrusions (Fig. 2*A*). To carry out further quantitative analysis, 2D maps of the on-rates were generated by counting the number of recruitment events per unit area (Fig. 2*B*). The 2D on-rate maps exhibited "hot" regions at the cell periphery, which also persist during expansion of a preexisting protrusion into broader lamellipodia (Fig. S2). Such dynamic membrane recruitment and distinct "hot" regions were not observed for the control construct, pm-Eos (Fig. 2 *C* and *D*). Statistical comparisons between pm-Eos and Eos-Rac1 were performed based on the coefficient of variance (CV) of the gray values of their respective 2D on-rate maps. A spatially regulated recruitment process is expected to yield a higher dispersion of the membrane on-rates and thus greater CV values. We found

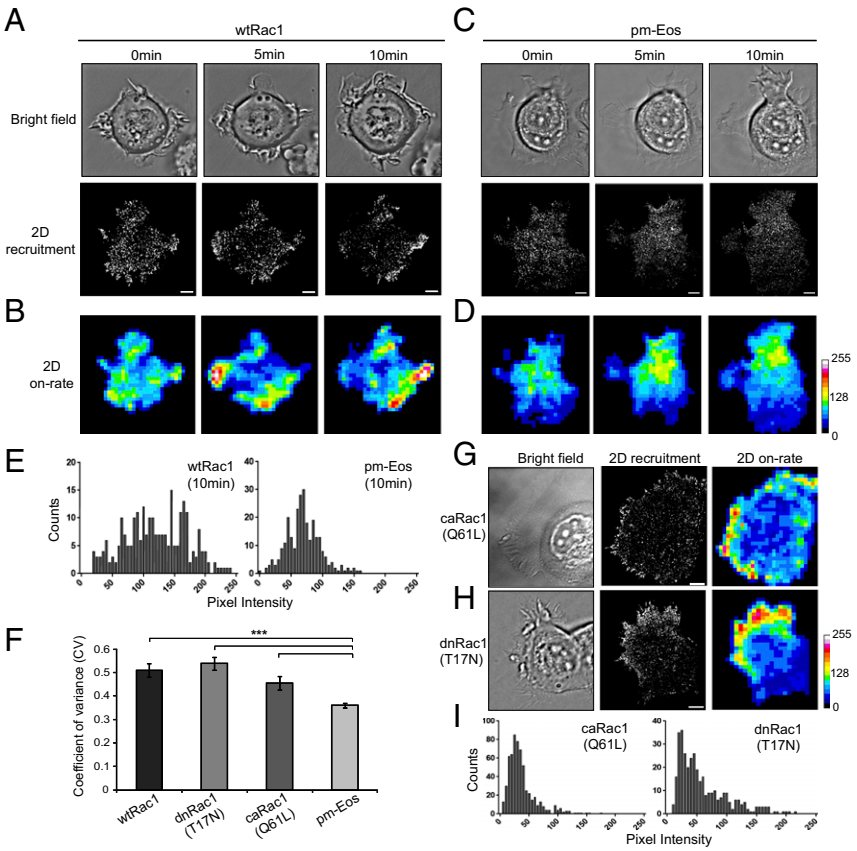

Fig. 2. Polarized recruitment of Rac1 to protrusions during cell spreading on collagen. MCF-7 cells expressing wtRac1 were allowed to spread on collagen-coated dishes and imaged thereafter. (*A*) Time series of an Eos-wtRac1 expressing cell exhibiting the formation of new protrusions (bright field panel). Corresponding 2D recruitment maps show polarized membrane binding of Rac1 to protrusion regions. (*B*) The 2D on-rate maps represent the binding events per area. Higher intensity indicates hot spots of increased recruitment/on-rates. (*C* and *D*) Bright field, 2D recruitment, and 2D on-rate maps of a pm-Eos expressing cell show no preferential Rac1 recruitment to protrusions. (*E*) Gray-value histograms calculated from 2D on-rate maps for both wtRac1 and pm-Eos expressing cell at 10-min time point. (*F*) Comparison of CV computed from 2D on-rate maps indicates the dispersion of the gray-value histograms of various constructs. (*G* and *I*) Bright field, 2D recruitment, and 2D on-rate maps for caRac1(Q61L) (*G*) and dnRac1(T17N) (*H*) expressing cells spreading on collagen, and the corresponding gray-value histograms (*I*). Scale bar corresponds to 5 μm. Error bars represent SEM for cells. ***$P < 0.001$. Values for each construct represent data pooled from several independent experiments, wtRac1 (10 cells, 5.8×10^4 trajectories), dnRac1 (7 cells, 4.1×10^4 trajectories), caRac1 (4 cells, 2.4×10^4 trajectories), and pm-Eos (6 cells, 3.0×10^4 trajectories).

that the CV values of Eos-Rac1 are significantly higher than that from the pm-Eos (Fig. 2 *E* and *F*).

We also performed the cell spreading experiment using cells expressing an Eos-tagged dominant negative Rac1 (T17N, dnRac1), or an Eos-tagged constitutively active Rac1 (Q61L, caRac1) mutants. In cell-expressing Eos-caRac1, the majority of the recruitment occurs in focal adhesion-like structures at the cell edge, in accordance with previous studies reporting Rac1 immobilization on focal adhesions (20) (Fig. 2*G*). Interestingly, although Eos-dnRac1-expressing cells did not form prominent lamellipodia-like protrusions, Eos-dnRac1 showed elevated membrane recruitment around the cell edge (Fig. 2*H*), leading to a broader distribution of on-rates than those from Eos-caRac1 (Fig. 2*I*). Therefore, the spatial regulation of membrane translocation of Rac1 is not directly dependent on the activation state or the nucleotide-bound state of the molecule.

Membrane Recruitment Is a Major Contributor to Polarized Rac1 Signaling. Elevated Rac1 recruitment directly contributes to polarized Rac1 signaling simply due to the increased molecular concentration at specific membrane regions. We estimated that the contrast due to recruitment, $\chi_{recruitment}$, defined as the ratio of the recruitment rate at the membrane protrusion of an "active" region to an "inactive" region, is about 2.1 ± 0.43 ($n = 15$), suggesting the contribution could be significant. On the other hand, spatial regulation of the GDP→GTP exchange process also promotes polarized Rac1 activation. To better understand the coordination of these two factors, we set out to image a Rac1 FRET sensor in conjunction with sptPALM analysis of Rac1 recruitment in the same cell. To simplify the experimental procedures, we used a modified Rac1 FRET sensor (Fig. 3*A*), which is modeled after previously published intramolecular FRET sensor designs, containing both the Rac1 sequence as well as a Rac1 binding domain (RBD) domain from PAK1 (16). The FRET donor is a CFP variant, Cerulean3 (Cer3), and the acceptor is mEos3.2 (26), which, in its green-emitting state, can accept energy transfer from Cer3 when the Rac1 domain is bound to the RBD (PAK1) domain (Fig. 3*A*). Meanwhile, a fraction of the mEos3.2 can be activated by UV illumination for SPT imaging. For controls, we also constructed a "constitutively active sensor" (RBD-caRac1), representing the high-FRET state of the sensor, as well as a "sensor" with a defective RBD domain (mutRBD-Rac1), representing the low-FRET state. We verified that RBD-caRac1 has a significant higher FRET ratio than mutRBD-Rac1 from the emission fluorescence spectra (Fig. 3*B*) as well as from whole-cell fluorescence measurements (Fig. S3*A*). The performance of the modified sensor was further validated by FRET ratiometric imaging in MCF-7 cells, which exhibited higher FRET ratios in the lamellipodia upon IGF1

stimulation, indicative of dynamic Rac1 activation (27), (Fig. S3*B* and Movie S3).

Next, we collected FRET images by TIRF illumination from cells during cell spreading, and carried out SPT experiments immediately after. As shown in Fig. 3*C*, regions with high Rac1 membrane recruitment also showed higher membrane FRET signals, indicating a high percentage of GTP-bound Rac1 (Fig. 3*C* and Movie S4). In contrast, a cell with no active protrusions or lamellipodia showed neither increased recruitment nor higher FRET activity (Fig. 3*D*). Therefore, our results suggest that Rac1 membrane targeting is spatially coupled to the nucleotide exchange process in cells and both contribute to polarization of Rac1 signaling. To evaluate the signaling contrast between the active and inactive regions due to the nucleotide exchange process, we converted the FRET ratiometric values, R, to a GTP-Rac1 fraction, η, which could be computed once the optical parameters of the two control constructs were characterized (*SI Text*). From there, we evaluated $\chi_{exchange}$, which is defined as

$$\chi_{exchange} = \eta_{active}/\eta_{inactive} = 1 + \left[\frac{\beta - 1}{R_T - R_D} + 1\right]^{-1} \frac{R_2 - R_1}{(R_1 - R_D)(R_2 - R_D)}$$

where R_T and R_D are the FRET ratios of RBD-caRac1 and mutRBD-Rac1, respectively, and $\beta = D_D/D_T$ is the relative brightness of the donor channel of the two control constructs (*SI Text*). We quantified the relative contributions of $\chi_{recruitment} - 1$ and $\chi_{exchange} - 1$ from the same cell (Fig. 3*E*), which shows correlation between these two measures of Rac1 activation. Furthermore, the distribution is skewed to the top half of the graph, suggesting that the membrane recruitment of Rac1 contributes significantly to the polarized Rac1 signaling, and is likely a factor no less important than the nucleotide exchange process. However, explicit evaluation of the relative contributions from the recruitment ratio and the nucleotide exchange ratio is impractical without a more detailed model that accounts for the dynamics of diffusion and dissociation.

Membrane Recruitment of Rac1 Precedes Interaction with Other Protein Factors. To understand the molecular mechanism of the membrane recruitment process, we performed extensive mobility analysis of the membrane-bound Rac1 molecules. Examination of individual molecular trajectories revealed that there are at least two subpopulations of Rac1 molecules with different diffusion rates (Fig. 4*A*). To quantify the heterogeneity, we computed histograms of molecular displacements (ΔT = 125 ms), (Fig. 4*B*), which showed two distinct peaks representing the two populations with different diffusion constants. The bimodal distribution was observed for wtRac1 as well as various Rac1 mutants (Table 1 and Fig. 4*B* illustrate all constructs). By fitting the displacement histogram with a bicomponent 2D diffusion model (19),

$$P^{[2]}(r) \sim C_1 r e x p\left(-\frac{r^2}{4D_1 t}\right) + C_2 r e x p\left(-\frac{r^2}{4D_2 t}\right),$$

we obtained the relative fraction of the two subpopulations, C_1 and C_2. The diffusion constants of the two subpopulations D_1

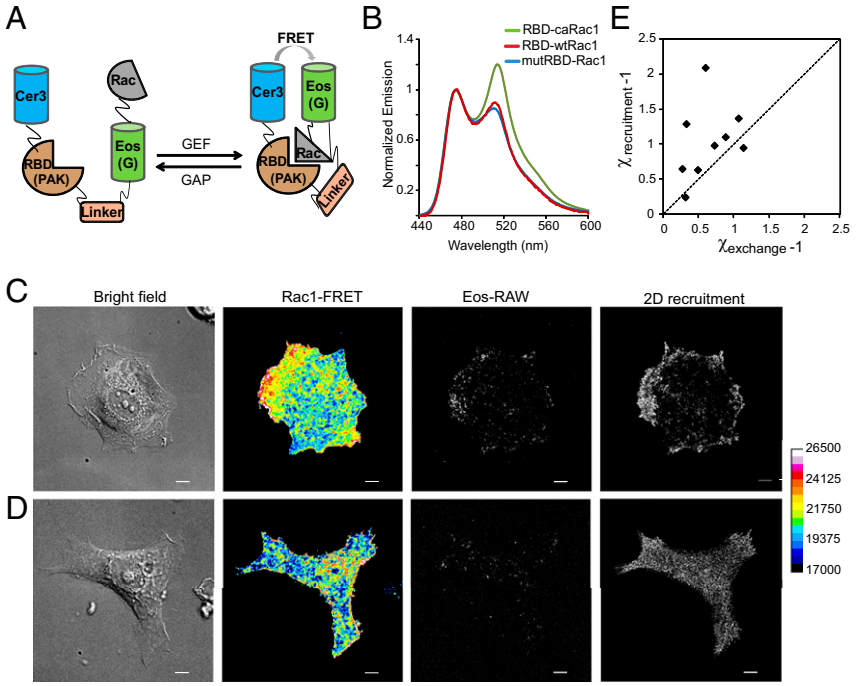

Fig. 3. Correlation between Rac1 activity and Rac1 membrane recruitment. MCF-7 cells expressing unimolecular Rac1 FRET sensor (RBD-Rac1) were allowed to spread on collagen, and coimaging of FRET and single-molecule Eos(SPT) was performed. (*A*) Design of the Rac1 FRET sensor used, with Cer3 as donor and mEos3.2 as acceptor. (*B*) Normalized emission spectra of Cer3 at 475 nm and green-emitting mEos3.2 at 510 nm as measured in 293HEK cells (36 h after transfection) with a fluorescence spectrophotometer by excitation with 430-nm light. Green, red, and blue lines correspond to "constitutively active" sensor (RBD-caRac1), "wild-type" sensor (RBD-Rac1), and "mutant" sensor (mutRBD-Rac1), respectively. Values represent average from triplicates. (*C*) Ratiometric (FRET/Cer3) TIRF images of the sensor show increased Rac1 activity in the lamellipodia region. Single molecules of Rac1 FRET sensor on the membrane (Eos-RAW) were detected by 543-nm excitation, and 2D recruitment maps were generated. Increased membrane recruitment of Rac1 correlate with higher FRET signal in the lamellipodia. (*D*) Images from an adherent MCF-7 cell without prominent lamellipodia show neither polarized Rac1-FRET signals nor polarized Rac1 membrane recruitment. Scale bar corresponds to 5 μm. Warmer colors indicate higher FRET. (*E*) Plot of recruitment polarization ($\chi_{recruitment} - 1$) versus exchange polarization ($\chi_{exchange} - 1$) from cells with sequential measurement of membrane FRET (exchange) and SPT (membrane recruitment). The dashed line represents an equal contribution from both the processes. Shown are 9 measurements from 7 cells.

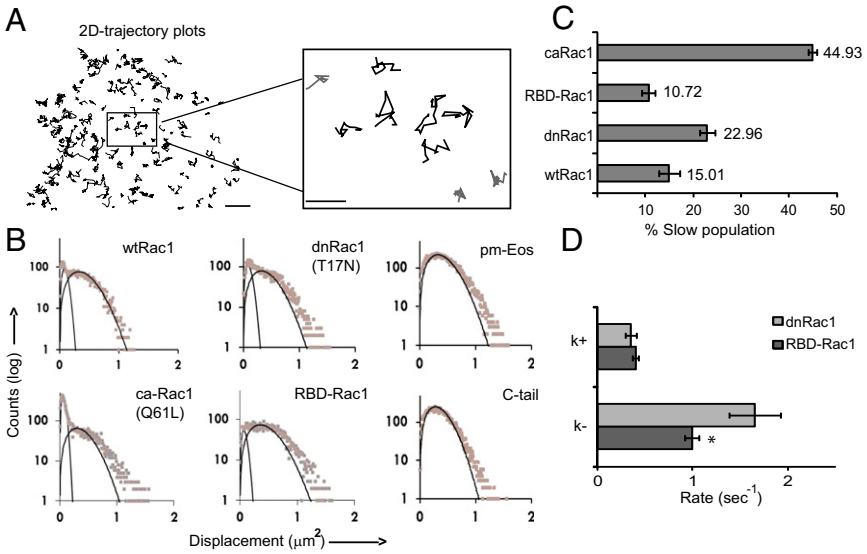

Fig. 4. Identification of heterogeneous diffusing populations in membrane-associated Rac1 molecules. MCF-7 cells expressing various Eos-Rac1 constructs and pm-Eos were imaged. (*A*) Single-molecule trajectories of Rac1 undergoing 2D lateral diffusion on the membrane. A high magnification view shows two types of trajectories: free diffusion (black) and confined diffusion/stationary (gray). (*B*) Histograms of 2D displacement ($\Delta T = 125$ ms) of the molecules were fitted with a bicomponent 2D diffusion model and the diffusion coefficients for the two populations calculated (Table 1). (*C*) Representative bar graph showing the percentage of molecules belonging to the slow diffusing (D_1) population for different Rac1 constructs. (*D*) Transition rates between the slow (D_1) and the fast diffusing (D_2) state, computed by HMM analysis of single-molecule trajectories. The graph represents the rates of association (k_+) and dissociation (k_-) from the slow (D_1) state. Scale bar corresponds to 5 μm. Error bars represent SEM for cells. $^*P < 0.05$. Values for each construct represent data pooled from several independent experiments wtRac1 (10 cells, 5.9×10^4 trajectories), dnRac1 (11 cells, 5.6×10^4 trajectories), caRac1 (9 cells, 5.0×10^4 trajectories), and RBD-Rac1 (9 cells, 4.4×10^4 trajectories).

and D_2 were also computed from the fitting and are summarized in Fig. 4*B* as well as in Table 1. The effective diffusion constant obtained from mean-square-displacement (MSD) analysis (Fig. S4) is between D_1 and D_2, as expected. In contrast, pm-Eos exhibited only one homogeneous diffusing population (Fig. 4*B*). Interestingly, the diffusion constant of pm-Eos is close to the D_2 (fast diffusion) of Rac1 constructs.

Binding of Rac1 to various protein factors, such as GEFs, GAPs, or downstream effectors, could slow down its diffusion and result in multiple diffusional populations. To test this hypothesis, we examined the mobility of Rac1 deletion mutant that contains only the tail sequence (Rac1 C-tail), which presumably does not interact with other protein factors. We found that indeed C-tail had only one homogeneous fast diffusion population (Fig. 4*B*), supporting this hypothesis. Further evidence was from more detailed analysis of Rac1 mobility on dnRac1 (T17N) as well as a chimeric construct of Rac1 (RBD-Rac1) containing the RBD from the Rac1-effector PAK1. Both of these constructs presumably interact primarily with GEFs—dnRac1 because it is incapable of exchanging GDP for GTP and RBD-Rac1 because the RBD is expected to suppress intermolecular interaction of Rac1 with other effectors. The RBD-Rac1 construct design is similar to that of previously described unimolecular Rac1 FRET sensors (Fig. 3*A* and Fig. S3*B*). We found that dnRac1 exhibits a higher D_1 fraction than RBD-Rac1 (Fig. 4*C*), consistent with the fact that dnRac1 traps GEFs in a tight binary complex (28–30). Furthermore, to evaluate the kinetics of interconversion between the two diffusive states (D_1 and D_2), we analyzed the SPT trajectories from dnRac1 and RDB-Rac1 with a two-state Hidden-Markovian model (HMM). The HMM analysis had been previously applied to single-molecule trajectories to study dimerization kinetics in growth factor receptors (31), protein-RNA interactions (32), and also integrin-cytoskeletal interactions (33). In our case, it allows us to extract the association and dissociation kinetics between Rac1 and its interacting GEFs. We found that indeed the complex form (D_1) and the free form (D_2) of Rac1 are interconverting at the time scale of milliseconds (for dissociation) to seconds (for association) (Fig. 4*D*). Furthermore, we found that the association rate (k_+) is similar for dnRac1 and RBD-Rac1 but the dissociation rate (k_-) is slower for dnRac1, consistent with a tighter binding for dnRac1 (28). Both the caRac1 and the wtRac1 also exhibited significant amounts of D_1 population (Fig. 4*C*), although quantitative modeling is difficult because they likely interact with a complex mixture of various protein factors. It should be noted that GEFs and Rac1 effectors are often themselves associated together as one large complex (34); therefore, complex formation with GEFs and with effectors may not be strictly separable events for wtRac. The results suggested that palmitoylation is not the reason for the two populations. Instead, our results suggested that the slow-diffusion state of Rac1 likely originated from protein–protein interactions.

An alternative explanation for the two diffusional populations is palmitoylation. It is recently reported that Rac1 is paltimoylated on Cys-178 (35); therefore the fast diffusion population could represent the unpalmitoylated Rac1 and the slow population could represent the palmitoylated ones. However, we found that the C178S mutant of Rac1 still retained this slow-diffusing population (Fig. S5), arguing against this explanation. The diffusion constants for both the fast and slow components for C178S

Table 1. Diffusion coefficients of slow (D_1) and fast (D_2) population from all Rac1 constructs

	D_1, μm²/s	D_2, μm²/s
wtRac1	0.020 ± 0.003	0.437 ± 0.029
dnRac 1 (T17N)	0.032 ± 0.003	0.420 ± 0.021
caRac1 (Q61L)	0.015 ± 0.004	0.361 ± 0.045
RBD-Rac1 chimera	0.017 ± 0.002	0.498 ± 0.053
C178S-Rac1	0.04 ± 0.002	1.075 ± 0.099
Rac1-C-tail		0.389 ± 0.091
pm-Eos		0.49 ± 0.035

mutant are about twice as fast as for wtRac (Table 1), potentially due to their lack of the palmitoylation.

We next set out to answer a mechanistic question concerning Rac1 recruitment: What is the initial state of Rac1 upon binding to the membrane? We consider two possibilities. First, Rac1 is recruited to the membrane via direct binding to lipid molecules. In this case, the Rac1 molecules should be initially in the fast-diffusing state, and their average mobility should decrease over time as the Rac1 molecules start to interact with other proteins. Alternatively, Rac1 is recruited by direct binding to another protein factor, e.g., a GEF molecule that is already localized to the plasma membrane. If the latter hypothesis is true, we would expect the average mobility of Rac1 to increase over time as it dissociates from the GEF-bound complex. We tested these predictions by aligning all SPT trajectories (obtained with higher time resolution, (ΔT = 45 ms) according to their initial recruitment point, and computing the average effective diffusion constants as a function of time. As shown in Fig. 5, in all Rac1 constructs we examined, we found that the effective diffusion constant decreased over time, supporting the first model (Fig. 5 *A*–*C*). As a control, we also carried out a similar analysis of freely diffusing pm-Eos, which, as expected, showed little change in effective diffusion constant as a function of time (Fig. 5*D*). This conclusion is further validated by fitting the data from dnRac1 (τ = 0.138 s) and RBD-Rac1(τ = 0.093 s) with single exponential decay functions, and back-extrapolating the fitting to obtain the diffusion constant at time 0 (time of the initial membrane binding). We obtain 0.4 $\mu m^2/s$ for dnRac1 and 0.59 $\mu m^2/s$ for RBD-Rac1, which are close to the values of D_2, representing the free Rac1 state. We observe that data from wtRac1 fit poorly with a single exponential decay, suggesting that interaction with downstream effectors can lead to more complicated changes in mobility. In conclusion, Rac1 is recruited to the membrane in a free unbound state but quickly reacts with other protein factors to reach an equilibrium population consisting of both free Rac1 and bound Rac1-complexes.

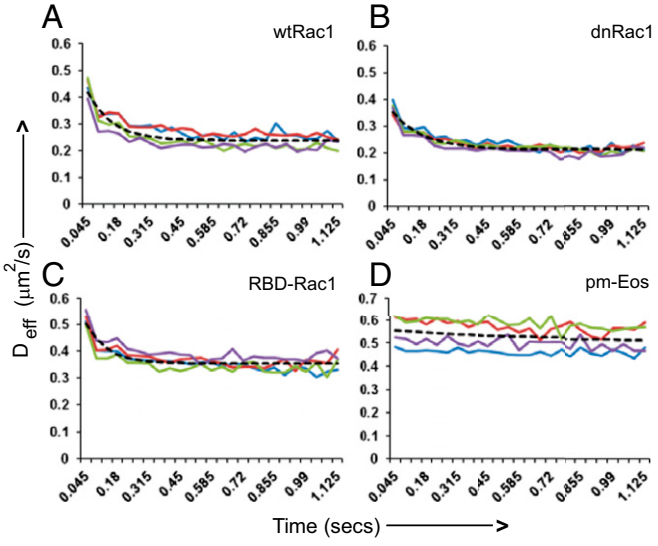

Fig. 5. Rac1 recruitment to membrane occurs in fast diffusing state. MCF-7 cells expressing Eos-wtRac1 (*A*), Eos-dnRac1 (*B*), Eos-RBD-Rac1 (*C*), or pmEos (*D*) were imaged with faster time resolution (ΔT = 45 ms). From all of the trajectories lasting ≥135 ms, the average effective diffusion coefficients were plotted as a function of time to determine the changes in mobility upon membrane binding. Each color represents a different cell. The graphs were fitted with a single exponential decay function (dashed line).

C-Term Hypervariable Region Is Important for the Regulation of Rac1 Recruitment. Our results thus far suggest Rac1 recruitment to plasma membrane is independent of its state of nucleotide loading or its switch regions, and is possibly mediated by binding to lipids. Studies have shown that the Rac1 binding to the plasma membrane requires prenylation of the C-terminal CAAX domain (7, 8, 36). However, the hypervariable (HV) region upstream of the CAAX sequence also modulates the subcellular localization of Rac1 (37, 38). The affinity of the polybasic sequences in the HV region of Rac1 to different phospholipids has been extensively studied in vitro (39–41). Therefore, we wanted to investigate if the HV region along with the CAAX domain from Rac1 is sufficient to recapitulate the spatially regulated Rac1 recruitment in live cells. We found that the construct encoding the HV+CAAX sequence from Rac1 (C-tail) localizes to cell nucleus primarily, with some distribution at cell membrane and cytosol (Fig. S6*A*), as was previously reported (35, 37, 38). TIR-FRAP (total internal reflection fluorescence recovery after photobleaching) analysis of the membrane fraction showed an average recovery time constant of 8.5 ± 0.68 s, indicating that the molecules are dynamically exchanging with the cytosolic pool (Fig. S6*B*). Consistent with this result, in sptPALM experiments, new molecules can be found to directly appear at the plasma membrane in the middle of the imaging field (Movie S5), indicating recruitment from cytosol. Based on the sptPALM data, we analyzed the recruitment rate of C-Tail during cell spreading, and indeed found that the molecules are specifically recruited to cell peripheral regions (Fig. 6*A*).

Further examination of the HV region of Rac1 (Fig. 6*F*) shows a short stretch of polyproline sequence (PPP) that mediates interaction with other protein factors (24, 42), as well as a short stretch of basic residues (RKR) that regulates its interaction with anionic phospholipids (39, 41, 43–45). To identify the specific sequences in HV critical for the spatial regulation of Rac1 recruitment, we generated mutants of Rac1 C-tail, by either mutating or deleting the poly-proline sequence (PPP > AAA, ΔPPP) or mutating the polybasic stretch (RKR > AAA) (Fig. 6*F*). We found that mutations of the basic residues (RKR > AAA) (Fig. 6*D*), but not of the polyproline sequence (PPP > AAA, ΔPPP) (Fig. 6 *B* and *C*), abolish the spatially regulated membrane recruitment. We use the CV values from 2D on-rate maps as a measure of polarized membrane translocation. Fig. 6*G* clearly demonstrates an increased Rac1 polarization in C-tail and PPP mutants versus the RKR > AAA mutant, which has a CV similar to pm-Eos. Another interesting feature of these Rac1-tail constructs is that their mobility does not change over time, most likely due to the fact that they do not engage in complex interactions with other protein factors (Fig. S7). These results further support the conclusion that Rac1 is recruited to the membrane by virtue of its C-terminal HV region via a direct interaction with the phospholipids, which accounts for both its initial free diffusive state and the spatial specificity of the process.

Spatial Regulation of Rac1 Membrane Recruitment by Localized PI (3,4,5)P_3 Synthesis. Existing studies suggest that the polybasic stretch on the C-terminal Rac1 tail may interact with the anionic phosphoinositide (3–5) triphosphate PI(3,4,5)P_3 in the membrane (44, 46). Based on the results from the previous section, we propose that the HV region of Rac1 can interact with PI (3,4,5)P_3 in the membrane, and this protein–lipid interaction is necessary and sufficient to drive polarized Rac1 membrane recruitment. We investigated whether the PI(3,4,5)P_3 gradient from the front to the back of cell protrusions correlates with the Rac1 gradient using ratiometric TIRF imaging. Both PI(3,4,5)P_3 and Rac1(C-tail and ΔPPP tail) levels closely parallel each other along the length of the protrusions (Fig. S8 *A* and *B*). Furthermore, reducing PI(3,4,5)P_3 levels using the PI3K inhibitor LY294002 (15 μM) led to reduced Rac1 in the leading front of

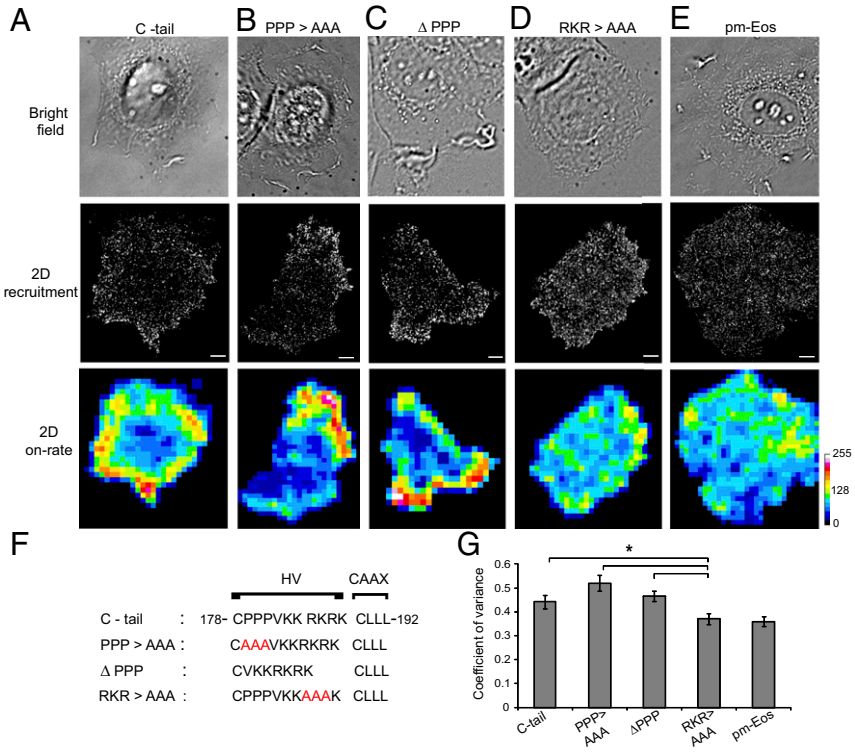

Fig. 6. C-terminal Hypervariable region regulates Rac1 recruitment. MCF-7 cells overexpressing Eos-labeled wild type and mutants of C-tail of Rac1 were imaged during spreading on collagen. (*A–E*) Bright field, 2D recruitment, and 2D on-rate maps show the membrane recruitment of C-tail (*A*), PPP > AAA (*B*), ΔPPP (*C*), RKR > AAA (*D*), and pm-Eos (*E*) molecule. Scale bar is 5 μm. (*F*) Sequences and the corresponding mutations of the C-terminal HV region of Rac1. (*G*) Representative graph shows the coefficient of variance for each construct, obtained from gray values of 2D on-rate maps. Error bars represent SEM for cells. $*P < 0.05$. Values for each construct represent data pooled from several independent experiments C-tail (6 cells, $n = 3.6 \times 10^4$ trajectories), PPP > AAA (6 cells, 3.7×10^4 trajectories), ΔPPP (5 cells, 2.9×10^4 trajectories), RKR > AAA (5 cells, 3.0×10^4 trajectories), and pm-Eos (6 cells, 2.8×10^4 trajectories).

the protrusions (Fig. S8 *D* and *E*), indicating that the polarization of Rac1 signaling in protrusions results from specific interaction with $PI(3,4,5)P_3$. Higher concentrations of the drug led to rounding-up of most of the cells (Fig. S8*C*), indicating the sensitivity of cell spreading process to PI3K inhibition.

Finally, to confirm that the spatially regulated membrane recruitment of Rac1 is a consequence of $PI(3,4,5)P_3$ polarization, we used an optogenetic strategy developed by Idevall-Hagren et al. that allows for optical manipulation of local $PI(3,4,5)P_3$ synthesis by inducing recruitment of PI3K to the plasma membrane (47). In this system, cells coexpressing CIBN-GFP-CAAX and the Cry2PHR-iSH2(p85α) were illuminated with blue light, which causes translocation of Cry2PHR-iSH2(p85α) associated with the endogenous p110α to the membrane and induces synthesis of $PI(3,4,5)P_3$. When a $PI(3,4,5)P_3$ probe, RFP-PH(Akt), was coexpressed in these cells, local blue-light illumination (440 nm) caused increased translocation of probe RFP-PH(Akt) to the plasma membrane near the illumination spot, indicating elevated local synthesis of $PI(3,4,5)P_3$ (Fig. 7*A* and Fig. S9 *A* and *B*). Local synthesis and accumulation of $PI(3,4,5)P_3$ also resulted in an active protrusion in some cases, consistent with the instructive role of $PI(3,4,5)P_3$ in activating actin pathways (48, 49).

To investigate the effect of local $PI(3,4,5)P_3$ synthesis on Rac1 membrane recruitment, we coexpressed the optogenetic constructs CIBN-GFP-CAAX, Cry2PHR-iSH2, together with Eos-labeled Rac1 tail constructs, C-tail and ΔPPP-tail, in MCF-7 cells. The Rac1 tail constructs were used to minimize the likelihood that protein–protein interaction, rather than the protein–lipid interaction, was responsible for light-induced polarization. Localized blue-light (440 nm, 10 ms) illumination of cells resulted in increased membrane recruitment of both C-terminal tail constructs, followed by generation of a new protrusion or expansion of a preexisting protrusion (Fig. 7 *B–E* and Movies S6 and S7). As a control, cells not expressing Cry2PHR-iSH2 did not exhibit significant increase in Rac1 recruitment (Fig. 7*F* and Movie S6) upon illumination with blue light. Furthermore, altering the site of illumination, and the resultant $PI(3,4,5)P_3$ distribution, effectively altered the spatial recruitment of Rac1 and the site of new protrusion generation (Fig. S9 *C–E* and Movies S8 and S9). These findings clearly demonstrate that spatial polarization of negatively charged $PI(3,4,5)P_3$ can directly lead to polarized Rac1 recruitment, and can explain the spatiotemporal regulation of Rac1 signaling and actin polymerization.

Discussion

In this study, we performed quantitative analysis of Rac1 recruitment to the plasma membrane using a single-particle tracking approach. We found that in spreading cells, the recruitment is not a purely passive process but is regulated spatially. The cellular regions that have higher levels of Rac1 activation also exhibit a higher rate of Rac1 recruitment, suggesting that plasma membrane recruitment and nucleotide exchange are coupled to generate stable cellular polarization. Our results indicated that the spatial regulation of the membrane recruitment rate is an important factor contributing to the spatial polarization of Rac1 signaling. This observation is in agreement with earlier studies (50), which showed that constitutively active Rac1 (independent of effector interactions) was recruited to the plasma membrane in a polarized manner.

Our study also unraveled the molecular mechanism behind Rac1 plasma membrane translocation, indicating the role of direct lipid binding, and further showed that the spatial regulation of recruitment is a consequence of asymmetric

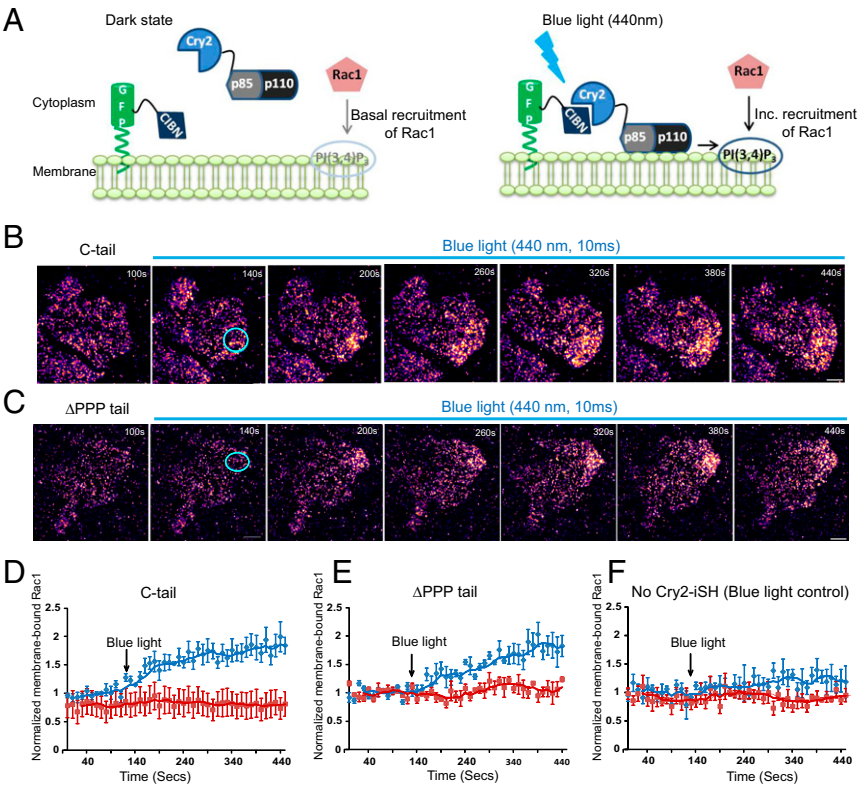

Fig. 7. Light-induced synthesis of PI(3,4)P_3 increases local membrane recruitment of Rac1. (*A*) Schematic of blue-light-induced dimerization of CIBN-CAAX and Cry2-iSH(p85α), resulting in plasma membrane recruitment of endogenous catalytic subunit p110α of PI3K. Subsequent activation of PI3K causes local synthesis of PI(3,4)P_3 at the membrane and increased Rac1 recruitment. (*B* and *C*) TIRF images of MCF-7 cells coexpressing CIBN-CAAX, Cry2-iSH, and Eos-Rac1 (C-tail and ΔPPP tail), before and during blue-light illumination. The pseudocolor represents membrane-bound single Rac1 molecules with higher-density regions showing brighter yellow colors. The blue circle indicates the area of blue-light illumination (440 nm, 10 ms), before acquiring each Eos image. (*D*–*F*) Representative graphs indicate the normalized membrane-bound Rac1 molecules before and after blue-light illumination for C-tail (*D*), ΔPPP tail (*E*), and cells lacking Cry2-iSH (blue-light control) (*F*) Blue line indicates the illuminated region, and red line indicates a region opposite to the illumination spot. Note that the number of membrane-bound Rac1 molecules does not change in the region away from the illumination. Scale bar corresponds to 10 μm. Error bars represent SEM for cells. Data pooled from three independent experiments. C-tail (5 cells), ΔPPP tail (5 cells), and blue-light control (4 cells).

phospholipid distribution on plasma membrane. Phospholipids are key signal mediators for cell polarization, and their intracellular distribution has been most well characterized in neutrophils and *Dictystelium* cells (3, 51, 52). Several lines of experimental evidences imply that phospholipid synthesis may coordinate with Rac1 activation to form a positive feedback loop; Rac1 signaling and Rac1 induced actin polymerization both affect the activities of PI3K, and in turn, the levels of PI(3,4,5)P_3 redistribute Rho GTPase activators such as DH-PH family GEFs on plasma membrane as well as affecting the catalytic activity of GEFs (3, 53, 54). Here we provide evidence for an additional mechanism of feedback: We show that the recruitment of Rac1 also plays an important role in this circuit and is regulated by the PI(3,4,5)P_3 levels. We may further speculate that PI(3,4,5)P_3 generation may be an upstream regulator for controlling the translocation of both Rac1 and the various DH-PH family GEFs, which results in a concerted polarization of Rac1 signaling in cells. In agreement with protein–lipid interactions playing a critical role in membrane targeting (44, 46, 55), our results show Rac1GTPase membrane localization may be primarily driven by lipids and not protein–protein interactions. This finding is consistent with previous studies in Rac1GTPases, which provide evidence that the membrane translocation can occur independent of GEF activation, e.g., caRac1 exhibiting polarized distribution in lamellipodia (50), and Rac1 membrane association occurring at the boundaries of rafts and lipid rafts followed by diffusion into the rafts for GEF-mediated activation (56). Similarly, in other RhoGTPases, like cdc42, the critical role of protein–lipid interactions (via the polybasic domain) in modulating cell growth and transformation has also been demonstrated (57).

The emergence of the sptPALM technique has made particle tracking in live cells relatively easy to implement (18, 19, 22). This approach has been used to study interactions between Rac1 and focal adhesions (20). Consistent with the fast 2D diffusion of membrane–associated Rac1 (20), our results also indicate that the majority of Rac1 exists in a freely diffusing state. We further show that sptPALM can be successfully implemented for accurate quantification of Rac1 membrane translocation processes. From the recruitment and on-rate maps, we are able to obtain dynamic information of the relative rates of membrane binding across the entire plasma membrane. The dynamic nature of "hot" regions of recruitment further implies that these on-rates are spatiotemporally regulated. Using statistical modeling of single-particle trajectories, we were able to decouple free Rac1 from its complex with GEFs/effectors and demonstrate that Rac1's membrane recruitment and nucleotide exchange occur in two consecutive steps. This finding helps to resolve a dichotomy in the field of RhoGTPases: whether membrane recruitment and activation by GEFs are coincident representing a single-step process (58) or are a two-step process (17, 59, 60). More recent studies on Rac1–lipid interactions showed that membrane association of Rac1 occurs preferentially at boundaries between ordered and disordered domains (56), which aligns well with our finding that mainly PI(3,4,5)P_3 (a nonlipid raft phospholipid)

regulate recruitment dynamics. Our assay with Rac1GTPase provides evidence that although membrane recruitment and GDP→GTP exchange are spatially correlated, temporally, these are independent and represent a sequential two-step process.

In comparison with traditional quantification of microscopy data, which typically relies on intensity measurements, quantification relying on particle counting/SPT offers certain advantages. The main advantage is that we can reliably and specifically identify membrane-bound molecules. Moreover, this technique is relatively insensitive to the fluorescent intensity fluctuation of individual molecules due to the digital nature of its quantification. The only disadvantage is that the density of molecules (and thus the dynamic range of the measurement) is limited; therefore some form of time averaging is usually required.

The plasma membrane not only serves as a boundary between the intracellular and extracellular milieus but also provides a necessary platform for biochemical reactions. Many cytosolic proteins transiently localize to the plasma membrane to carry out their functions. These include small GTPases, various adaptor molecules for surface receptors and cytosolic kinases, and many others. The experimental strategy used in this study is reasonably general in its approach and simple in its instrumentation, and thus can be applied to many of these proteins.

Materials and Methods

Plasmids. Entry clones of the different Rac1 plasmids (wt, T17N, Q61L) were generated using PCR fragments of the respective Rac1 using the pENTR/D-TOPO cloning system (Invitrogen). The cDNAs of Rac1 and its mutants were generous gifts of Klaus Hahn (University of North Carolina at Chapel Hill, Chapel Hill, NC). A tdEos-gateway vector was created by inserting the gateway cassette (Invitrogen) into the C terminus of the pRSET-A/tdEos vector (obtained from Adgene Inc.). The Rac1 sequence was subcloned into the tdEos gateway vector using the LR clonase II (Invitrogen), following manufacturer's instructions, to produce the Eos-Rac1 fusion constructs. For the various Rac1 C-terminal tail constructs, the entry clones were prepared from hybridized DNA sequences corresponding to the respective tail domains. Gateway cloning between the Rac-tail entry clones and mCherry-gateway vectors was also done to generate mCherry-C tail, and mCherry-ΔPPP tail. A volume marker mCer3-C1 was used for ratiometric imaging.

The unimolecular Rac1 FRET sensor was adapted from an unpublished FRET sensor of Rac1. Similar to the published RhoA sensor (16), a RBD derived from PAK1 was used to sense the nucleotide state of Rac1. Rac1 is located at the C terminus of the sensor to preserve its proper interaction with RhoGDI and other proteins. To be compatible with single-particle tracking, the sensor employs Cerulean3 as the FRET donor and mEos3.2 as the FRET acceptor. Variants of the sensor included mutant sensor with the mutation H83,86D in the RBD of PAK1 (mutRBD-wtRac1) and constitutively active sensor with caRac1(Q61L) (RBD-caRac1).

The pm-Eos clone was constructed by inserting the sequence corresponding to the membrane-targeting peptide (MGCIKSKRKDNLNDDE) from Lyn kinase into the N terminus of the Eos coding sequence. Expression vectors encoding the inter-SH2 (iSH2) domain of regulatory subunit (p85α) fused with the PHR domain of Cry2 (Cry2-iSH2), and the $PI(3,4,5)P_3$ probe RFP-PH(Akt), and EGFP-PH(Akt) were kind gifts from Pietro DeCamilli's laboratory (Yale University, New Haven, CT) (47). CIBN-CAAX plasmid was obtained from Addgene.

Cell Culture and Transfection. Breast carcinoma MCF-7 cells were maintained in DMEM supplemented with 10% (vol/vol) FBS under 5% CO_2. Cells plated onto 35-mm plastic dishes were transfected with 400 ng of DNA using 1.5 μL of Lipofectamine 2000 (Invitrogen) for 6 h. Following that, cells were either plated on plasma-cleaned glass-bottom dishes (MatTek) or allowed to grow before plating on collagen-coated glass-bottom dishes. A 0.03% solution of type I Collagen from rat tail (Invitrogen) was prepared in 0.02 M Acetic acid. Replating was done at around 50% confluence to achieve imaging of isolated cells.

Pulldown Assay. Eos-Rac1 constructs (wt, dn, and ca) were coexpressed with FLAG-tagged PAK in HEK293 cells by transient transfection with JetPrime reagent (Polyplus Transfection). Twenty-four hours after transfection, the cells were lysed in 50 mM Tris pH 7.5, 150 mM NaCl, and 1% Triton X-100 (lysis buffer) with addition of EDTA-free protease inhibitor mixture (Sigma). The supernatants collected after centrifugation were incubated with Flag/M2-agarose beads (Sigma) for 1 h at 4 °C. Following that, the beads were washed, and eluted with lysis buffer containing 200 μg mL^{-1} 3×Flag peptide (Sigma). The eluted protein complexes and cell lysates were fractionated on 4–12% (wt/vol) NuPAGE gels (Invitrogen) followed by Western blot analysis using antibodies against Rac1 (23A8, Millipore) and PAK (*N*-20, Santa Cruz).

Microscopy and Image Analysis.

sptPALM. Single-molecule fluorescence images were taken with a modified epifluorescence microscope (Olympus IX81) equipped with 60× TIRF objective (numerical aperture = 1.49, Olympus) and a thermoelectric-cooled EM-CCD camera (PhotonMax, Roper Scientific). Both wide-field and TIRF illumination were used for the study. For photoactivation of Eos molecules, a 405-nm diode laser (Cube laser system, Coherent Inc.) was used, and the activation pulse was controlled as described previously (19, 22). The green fluorescence of unactivated Eos was excited with the 488-nm laser line from an argon ion laser (Melles Griot). Single-molecule imaging of activated Eos molecules was performed with a 562-nm DPSS laser (Crystal Lasers). The angle of the laser was changed using a step motor (Thor Labs, Inc.) to achieve the critical angle for TIRF illumination.

Unless otherwise stated, single-molecule time-lapse images were obtained under continuous illumination with 120-ms acquisition time for each image. Image acquisition software was built on top of μManager platform. By setting the exposure time to about 125 ms, membrane-bound Rac1 molecules can be detected, appearing as transient, diffraction-limited fluorescence spots that were easily identifiable from much weaker and diffuse fluorescent signals from within the cytoplasm. The signal from the cytosolic fraction of the molecules was partially filtered by a particle detection algorithm due to its irregular, non-Gaussian signal profile. The images were analyzed using an automated particle tracking algorithm as described previously (61). The PSF of the diffraction-limited spot is fitted to a Gaussian kernel, and the centroid position of the spot is tracked over time to generate spatiotemporal trajectories of each detected spot. Based on single-molecule trajectories, those molecules that underwent 2D random motion were considered membrane bound and retained. Molecules that appeared only transiently in the TIRF illumination field and disappeared within 375 ms were indicative of 3D diffusion and therefore not counted.

The 2D recruitment and PALM maps were generated, respectively, from the initial centroid position and all of the centroid positions of single-molecule trajectories. Averaging pixels (scaling down 10-fold) from 2D recruitment maps gave rise to 2D on-rate maps, where each pixel represents $1.6 \times 1.6\ \mu m^2$ grids. The 2D on-rate maps indicate the rate of recruitment events per cell area. The 2D on-rate maps were further processed with a Gaussian blur filter (0.5 pixels) on Image J for better representation. The gray value of each pixel in the 2D on-rate map was computed and plotted as a histogram. The CV indicating the dispersion (broadness) of the distribution was computed across many cells by dividing the SD of the distribution by mean intensity gray value.

HMM analysis of the particle tracking data are carried out with a modified version of the vbSPT program (sourceforge.net/projects/vbspt/) originally developed by Persson et al. (32). The results were computed on a 128-node Matlab distributed computing server. Only results from a two-state model were used. Model comparison was not performed.

FRET Imaging. FRET imaging was performed on an inverted microscope (customized from Nikon Ti-E) with a 60× TIRF objective (numerical aperture = 1.49). Images were captured by an iXon Ultra EM-CCD (Andor, Oxford Instruments). During imaging, the cells were maintained in a heated chamber (37 °C) supplemented with 5% CO_2. For wide-field FRET imaging, excitation was achieved with a LED light source (Lumencor), and images were acquired with 300-ms exposure time at 1-min intervals for both Cer(CFP) and GFP channels. For co-imaging of FRET and single molecules under TIRF illumination, donor (Cer) was excited with a 442-nm DPSS laser (Crystal Lasers) and activated Eos molecules were excited using a 543-nm DPSS laser. The activation of Eos was performed with a 405-nm LED lamp (ThorLabs) using the external trigger mode of the Andor iXon Ultra. TIRF FRET images were acquired using a 400-ms exposure for both Cer and GFP channels with a 10-s interval. Immediately after, time-lapse images of single molecules were acquired under continuous acquisition with a 100-ms exposure time. The imaging software was built on the MetaMorph platform and the ratiometric image analysis was performed on MetaMorph.

TIRF Imaging. Time-lapse TIRF imaging was performed for cells using Nikon Ti-E microscope under above-mentioned conditions. Sequential images of Cer, GFP, and mCherry were captured every 2 min using excitation with 442-nm, 505-nm, and 594-nm DPSS lasers (Crystal Lasers). Ratiometric images EGFP/Cer or mCherry/Cer were generated. Protruding regions of cells were identified, and a band scan of 5 μm width was done to measure the intensity profile

along the protrusion. The values were normalized to those at back of the protrusion (averaging the rearmost five pixels), and their log values were plotted for the entire length of protrusion.

Optogenetic Control of PI(3,4,5)P_3 Synthesis. Spatially controlled blue light (440 nm) was delivered through the Mosaic illumination system (Andor, Inc.) to the Nikon Ti-E microscope. Images for RFP-PH(Akt) or Eos-Rac1 were acquired every 10 s, with a 594-nm or 543-nm laser line, respectively, under TIRF illumination. After baseline acquisition, a short blue pulse (440 nm, 10 ms) was delivered before acquiring each RFP-PH(Akt) or Eos-Rac1 image.

Statistical Analysis. Averages and SEMs were calculated and are shown in the respective graphs. The indicated *P* values were obtained from one-tailed Student's *t* tests.

ACKNOWLEDGMENTS. We thank Prof. Pietro DeCamilli (Yale University) for the generous gifts of the Cry2-iSH2, RFP-PH(Akt), and EGFP-PH(Akt) constructs. We sincerely thank Prof. Ann Cowan (University of Connecticut Health Center) for her critical reading of the manuscript. The research is supported by National Institute of Health Grants R01GM085301 (to J.Y.) and R21NS071216 (to Y.I.W.).

1. Nobes CD, Hall A (1999) Rho GTPases control polarity, protrusion, and adhesion during cell movement. *J Cell Biol* 144(6):1235–1244.
2. Ridley AJ (2001) Rho GTPases and cell migration. *J Cell Sci* 114(Pt 15):2713–2722.
3. Weiner OD, et al. (2002) A PtdInsP(3)- and Rho GTPase-mediated positive feedback loop regulates neutrophil polarity. *Nat Cell Biol* 4(7):509–513.
4. Park KC, et al. (2004) Rac regulation of chemotaxis and morphogenesis in *Dictyostelium*. *EMBO J* 23(21):4177–4189.
5. Jaffe AB, Hall A (2005) Rho GTPases: Biochemistry and biology. *Annu Rev Cell Dev Biol* 21:247–269.
6. Garcia-Mata R, Boulter E, Burridge K (2011) The 'invisible hand': Regulation of RHO GTPases by RHOGDIs. *Nat Rev Mol Cell Biol* 12(8):493–504.
7. Roberts PJ, et al. (2008) Rho Family GTPase modification and dependence on CAAX motif-signaled posttranslational modification. *J Biol Chem* 283(37):25150–25163.
8. Bustelo XR, Ojeda V, Barreira M, Sauzeau V, Castro-Castro A (2012) Rac-ing to the plasma membrane: The long and complex work commute of Rac1 during cell signaling. *Small GTPases* 3(1):60–66.
9. Boulter E, Garcia-Mata R (2010) RhoGDI: A rheostat for the Rho switch. *Small GTPases* 1(1):65–68.
10. DerMardirossian C, Bokoch GM (2005) GDIs: Central regulatory molecules in Rho GTPase activation. *Trends Cell Biol* 15(7):356–363.
11. Dransart E, Morin A, Cherfils J, Olofsson B (2005) Uncoupling of inhibitory and shuttling functions of rho GDP dissociation inhibitors. *J Biol Chem* 280(6):4674–4683.
12. Hoffman GR, Nassar N, Cerione RA (2000) Structure of the Rho family GTP-binding protein Cdc42 in complex with the multifunctional regulator RhoGDI. *Cell* 100(3): 345–356.
13. Machacek M, et al. (2009) Coordination of Rho GTPase activities during cell protrusion. *Nature* 461(7260):99–103.
14. Itoh RE, et al. (2002) Activation of rac and cdc42 video imaged by fluorescent resonance energy transfer-based single-molecule probes in the membrane of living cells. *Mol Cell Biol* 22(18):6582–6591.
15. Pertz O (2010) Spatio-temporal Rho GTPase signaling—Where are we now? *J Cell Sci* 123(Pt 11):1841–1850.
16. Pertz O, Hodgson L, Klemke RL, Hahn KM (2006) Spatiotemporal dynamics of RhoA activity in migrating cells. *Nature* 440(7087):1069–1072.
17. Moissoglu K, Slepchenko BM, Meller N, Horwitz AF, Schwartz MA (2006) In vivo dynamics of Rac-membrane interactions. *Mol Biol Cell* 17(6):2770–2779.
18. Manley S, et al. (2008) High-density mapping of single-molecule trajectories with photoactivated localization microscopy. *Nat Methods* 5(2):155–157.
19. Niu L, Yu J (2008) Investigating intracellular dynamics of FtsZ cytoskeleton with photoactivation single-molecule tracking. *Biophys J* 95(4):2009–2016.
20. Shibata AC, et al. (2013) Rac1 recruitment to the archipelago structure of the focal adhesion through the fluid membrane as revealed by single-molecule analysis. *Cytoskeleton* 70(3):161–177.
21. Wiedenmann J, et al. (2004) EosFP, a fluorescent marker protein with UV-inducible green-to-red fluorescence conversion. *Proc Natl Acad Sci USA* 101(45):15905–15910.
22. Oh D, et al. (2012) Fast rebinding increases dwell time of Src homology 2 (SH2)-containing proteins near the plasma membrane. *Proc Natl Acad Sci USA* 109(35): 14024–14029.
23. Zacharias DA, Violin JD, Newton AC, Tsien RY (2002) Partitioning of lipid-modified monomeric GFPs into membrane microdomains of live cells. *Science* 296(5569): 913–916.
24. ten Klooster JP, Jaffer ZM, Chernoff J, Hordijk PL (2006) Targeting and activation of Rac1 are mediated by the exchange factor beta-Pix. *J Cell Biol* 172(5):759–769.
25. Choma DP, Pumiglia K, DiPersio CM (2004) Integrin $\alpha3\beta1$ directs the stabilization of a polarized lamellipodium in epithelial cells through activation of Rac1. *J Cell Sci* 117(Pt 17):3947–3959.
26. Zhang M, et al. (2012) Rational design of true monomeric and bright photoactivatable fluorescent proteins. *Nat Methods* 9(7):727–729.
27. Haase I, Evans R, Pofahl R, Watt FM (2003) Regulation of keratinocyte shape, migration and wound epithelialization by IGF-1- and EGF-dependent signalling pathways. *J Cell Sci* 116(Pt 15):3227–3238.
28. Feig LA (1999) Tools of the trade: Use of dominant-inhibitory mutants of Ras-family GTPases. *Nat Cell Biol* 1(2):E25–E27.
29. García-Mata R, et al. (2006) Analysis of activated GAPs and GEFs in cell lysates. *Methods Enzymol* 406:425–437.
30. Wong KW, Mohammadi S, Isberg RR (2006) Disruption of RhoGDI and RhoA regulation by a Rac1 specificity switch mutant. *J Biol Chem* 281(52):40379–40388.
31. Chung I, et al. (2010) Spatial control of EGF receptor activation by reversible dimerization on living cells. *Nature* 464(7289):783–787.
32. Persson F, Lindén M, Unoson C, Elf J (2013) Extracting intracellular diffusive states and transition rates from single-molecule tracking data. *Nat Methods* 10(3):265–269.
33. Das R, Cairo CW, Coombs D (2009) A hidden Markov model for single particle tracks quantifies dynamic interactions between LFA-1 and the actin cytoskeleton. *PLOS Comput Biol* 5(11):e1000556.
34. Rossman KL, Der CJ, Sondek J (2005) GEF means go: Turning on RHO GTPases with guanine nucleotide-exchange factors. *Nat Rev Mol Cell Biol* 6(2):167–180.
35. Navarro-Lérida I, et al. (2012) A palmitoylation switch mechanism regulates Rac1 function and membrane organization. *EMBO J* 31(3):534–551.
36. Clarke S (1992) Protein isoprenylation and methylation at carboxyl-terminal cysteine residues. *Annu Rev Biochem* 61:355–386.
37. Michaelson D, et al. (2001) Differential localization of Rho GTPases in live cells: Regulation by hypervariable regions and RhoGDI binding. *J Cell Biol* 152(1):111–126.
38. Lam BD, Hordijk PL (2013) The Rac1 hypervariable region in targeting and signaling: A tail of many stories. *Small GTPases* 4(2):78–89.
39. Ugolev Y, Molshanski-Mor S, Weinbaum C, Pick E (2006) Liposomes comprising anionic but not neutral phospholipids cause dissociation of Rac(1 or 2) x RhoGDI complexes and support amphiphile-independent NADPH oxidase activation by such complexes. *J Biol Chem* 281(28):19204–19219.
40. Ugolev Y, Berdichevsky Y, Weinbaum C, Pick E (2008) Dissociation of Rac1(GDP). RhoGDI complexes by the cooperative action of anionic liposomes containing phosphatidylinositol 3,4,5-trisphosphate, Rac guanine nucleotide exchange factor, and GTP. *J Biol Chem* 283(32):22257–22271.
41. Finkielstein CV, Overduin M, Capelluto DG (2006) Cell migration and signaling specificity is determined by the phosphatidylserine recognition motif of Rac1. *J Biol Chem* 281(37):27317–27326.
42. van Hennik PB, et al. (2003) The C-terminal domain of Rac1 contains two motifs that control targeting and signaling specificity. *J Biol Chem* 278(40):39166–39175.
43. Williams CL (2003) The polybasic region of Ras and Rho family small GTPases: A regulator of protein interactions and membrane association and a site of nuclear localization signal sequences. *Cell Signal* 15(12):1071–1080.
44. Heo WD, et al. (2006) PI(3,4,5)P3 and PI(4,5)P2 lipids target proteins with polybasic clusters to the plasma membrane. *Science* 314(5804):1458–1461.
45. Magalhaes MA, Glogauer M (2010) Pivotal Advance: Phospholipids determine net membrane surface charge resulting in differential localization of active Rac1 and Rac2. *J Leukoc Biol* 87(4):545–555.
46. Missy K, et al. (1998) Lipid products of phosphoinositide 3-kinase interact with Rac1 GTPase and stimulate GDP dissociation. *J Biol Chem* 273(46):30279–30286.
47. Idevall-Hagren O, Dickson EJ, Hille B, Toomre DK, De Camilli P (2012) Optogenetic control of phosphoinositide metabolism. *Proc Natl Acad Sci USA* 109(35):E2316–E2323.
48. Insall RH, Weiner OD (2001) PIP3, PIP2, and cell movement—Similar messages, different meanings? *Dev Cell* 1(6):743–747.
49. Xu J, et al. (2003) Divergent signals and cytoskeletal assemblies regulate self-organizing polarity in neutrophils. *Cell* 114(2):201–214.
50. Del Pozo MA, et al. (2002) Integrins regulate GTP-Rac localized effector interactions through dissociation of Rho-GDI. *Nat Cell Biol* 4(3):232–239.
51. Funamoto S, Milan K, Meili R, Firtel RA (2001) Role of phosphatidylinositol 3′ kinase and a downstream pleckstrin homology domain-containing protein in controlling chemotaxis in *Dictyostelium*. *J Cell Biol* 153(4):795–810.
52. Chung CY, Funamoto S, Firtel RA (2001) Signaling pathways controlling cell polarity and chemotaxis. *Trends Biochem Sci* 26(9):557–566.
53. Welch HC, Coadwell WJ, Stephens LR, Hawkins PT (2003) Phosphoinositide 3-kinase-dependent activation of Rac. *FEBS Lett* 546(1):93–97.
54. Yang HW, et al. (2012) Cooperative activation of PI3K by Ras and Rho family small GTPases. *Mol Cell* 47(2):281–290.
55. Yeung T, et al. (2008) Membrane phosphatidylserine regulates surface charge and protein localization. *Science* 319(5860):210–213.
56. Moissoglu K, et al. (2014) Regulation of Rac1 translocation and activation by membrane domains and their boundaries. *J Cell Sci* 127(Pt 11):2565–2576.
57. Johnson JL, Erickson JW, Cerione RA (2012) C-terminal di-arginine motif of Cdc42 protein is essential for binding to phosphatidylinositol 4,5-bisphosphate-containing membranes and inducing cellular transformation. *J Biol Chem* 287(8):5764–5774.
58. Bokoch GM, Bohl BP, Chuang TH (1994) Guanine nucleotide exchange regulates membrane translocation of Rac/Rho GTP-binding proteins. *J Biol Chem* 269(50): 31674–31679.
59. Fauré J, Vignais PV, Dagher MC (1999) Phosphoinositide-dependent activation of Rho A involves partial opening of the RhoA/Rho-GDI complex. *Eur J Biochem* 262(3): 879–889.
60. del Pozo MA, et al. (2004) Integrins regulate Rac targeting by internalization of membrane domains. *Science* 303(5659):839–842.
61. Tatavarty V, Kim EJ, Rodionov V, Yu J (2009) Investigating sub-spine actin dynamics in rat hippocampal neurons with super-resolution optical imaging. *PLoS ONE* 4(11): e7724.